

1 **Dissolved oxygen as indicator of multiple drivers of the marine** 2 **ecosystem: the Southern Adriatic Sea case study**

3 Valeria Di Biagio¹, Riccardo Martellucci¹, Milena Menna¹, Anna Teruzzi¹, Carolina Amadio¹, Elena
4 Mauri¹, Gianpiero Cossarini¹

5 ¹National Institute of Oceanography and Applied Geophysics - OGS, Trieste, Italy

6 *Correspondence to:* Valeria Di Biagio (vdibiagio@ogs.it)

7 **Abstract.** Oxygen is essential to all aerobic organisms and its dynamics in the ocean involve interconnected physical and
8 biological processes that are at the basis for the marine ecosystem functioning. The study of dissolved oxygen (DO) variations
9 under multiple drivers is currently one of the main goals of climate and marine ecological scientific communities, and the
10 quantification of DO levels is essential for the assessment of the environmental status, especially in coastal areas.

11 We investigate the 1999-2021 interannual variability of DO in the southern Adriatic Sea, a marginal area of the Mediterranean
12 Sea, where deep water formation processes occur, contributing significantly to the ventilation of the Eastern Mediterranean
13 basin. Following the Marine Strategy Framework Directive, which promotes the integration of different observational
14 platforms, we use DO modelled by the Copernicus Marine Mediterranean Sea biogeochemical reanalysis, which assimilates
15 satellite chlorophyll concentrations and to which we apply a bias correction using DO Argo float measurements in 2014-2020.
16 A correlation analysis of the time series of the first three modes of variability (86% of the total variance) of the DO profiles
17 extracted from the bias-corrected reanalysis with key meteo-marine indicators shows a link with (i) net heat fluxes related to
18 oxygen solubility, (ii) vertical mixing, (iii) biological production at the surface and in subsurface layers, and (iv) circulation
19 associated with the entrance of northern Adriatic waters. The alternating entrance of Levantine and Atlantic Waters through
20 the North Ionian Gyre (NIG) appears to be the driver of the fourth mode of variability, which explains 8% of the total variance.
21 Moreover, we find that the first temporal mode of variability is the main driver of the negative anomaly of DO in the 0-600 m
22 layer in 2021 with respect to the 1999-2020 climatology. We ascribe the lower content of DO in 2021 to a negative anomaly
23 of the subsurface biological production in the same year, in agreement with the previous correlation analysis, but not to heat
24 fluxes. Indeed, in agreement with previous studies, we observe a sharp increase in salinity favoured by the cyclonic circulation
25 of NIG from 2019 onwards. We interpret this as a possible regime shift that is not captured by the time series analysis, and
26 whose possible consequences for Ionian-Adriatic system ventilation and for marine organisms should be carefully monitored
27 in the near future.

28 **1 Introduction**

29 Dissolved oxygen (DO) is a key indicator for monitoring the marine ecosystem functioning, because it is the result of several
30 atmospheric, hydrodynamic and biogeochemical driving processes (such as air-sea fluxes, vertical convection and mixing,
31 horizontal transport, biological production and consumption; Keeling and Garcia, 2002; Oschlies et al., 2018; Pitcher et al.,
32 2021). Indeed, DO is currently being studied under the global warming scenarios by climate and marine ecological scientific
33 communities (e.g. Pörtner et al., 2019; Kwiatkowski et al., 2020; Garcia-Soto et al., 2021), as oxygen depletion has been
34 observed in the global ocean as well as at local scale (Breitburg et al., 2018). Climate models predict a reduction in global
35 ocean dissolved oxygen content (Matear et al., 2000; Oschlies et al., 2008; Stramma et al., 2010, Reale et al., 2021), so this
36 parameter is of primary interest especially in those areas where oceanic processes connect surface and deep layers.

37 The southern Adriatic Sea (SAdr, Fig. 1a) is one of these areas, as it is an area of deep water formation (Gačić et al., 2002;
38 Pirro et al., 2022) and represents the deep engine of the eastern Mediterranean thermohaline circulation (Malanotte-Rizzoli et
39 al., 1999), which is crucial for the eastern basin ventilation. The Adriatic Sea (Fig. 1a) is an elongated, semi enclosed and
40 roughly north-south oriented basin characterized by a shallow northern shelf (shallower than 80 m) and a deep pit in its southern
41 part (maximum depth of approximately 1200 m) which is connected to the Ionian Sea (central Mediterranean basin) through
42 the Otranto Strait (with a maximum depth of 800 m). The Adriatic Sea is characterized by a cyclonic circulation governed by
43 several drivers: river runoff, wind stress, surface buoyancy fluxes and mass exchanges through the Otranto Strait (Cushman-
44 Roisin et al., 2013).

45 The SAdr is strongly influenced by the inflow of water masses from the northern Adriatic Sea (i.e., North Adriatic Dense
46 Water, Querin et al., 2016) and the Ionian Sea. In particular, the inflow of southern water masses is triggered by the periodic
47 reversal of Northern Ionian Gyre circulation (Gačić et al., 2002; Civitarese et al., 2010, Menna et al., 2019). This oscillating
48 system, called the Adriatic - Ionian Bimodal Oscillating System (BiOS), changes the circulation of the Northern Ionian Gyre
49 from cyclonic to anticyclonic and vice versa, modulating the advection of water masses in the Adriatic Sea (Gačić et al., 2010,
50 Rubino et al., 2020). The cyclonic circulation of the Northern Ionian Gyre causes the advection of saline water masses of
51 Levantine origin (i.e., Levantine Intermediate Water, Cretan Intermediate Water, Ionian Surface Water and Levantine Surface
52 Water, Manca et al., 2006), while the anticyclonic circulation favours the inflow of Atlantic water and a relative decrease of
53 salinity in the SAdr (Gačić et al., 2011, Menna et al., 2022a). This feature has a strong influence on the biogeochemical
54 properties of the SAdr, affecting nutrient availability (Civitarese et al., 2010), phytoplankton blooms (Gačić et al., 2002;
55 Civitarese et al., 2010), and species composition (Batistić et al., 2014, Mauri et al., 2021).

56 While hydrodynamic and biogeochemical properties of SAdr have been widely described in several studies (e.g., Civitarese et
57 al. 2010; Cushman-Roisin et al., 2013; Lipizer et al., 2014; Kokkini et al., 2018, 2019; Mavropoulou et al., 2020; Mihanović
58 et al., 2021; Menna et al., 2022b), at the best of our knowledge DO dynamics in the area in connection with relevant driving
59 processes over decadal time scales have not been addressed yet.

60 Investigating the DO multidecadal variability is crucial for quantifying the state of the marine environment (Marine Strategy
61 Framework Directive, MSFD; Oesterwind et al., 2016) and for understanding anthropogenic impacts on the marine
62 environment (Pörtner et al., 2022). The emerging ecosystem-based management method proposed by the MSFD (2008/56/EC)
63 promotes the use of different observational platforms, allowing to synoptically collect information on the space-time
64 distribution of important parameters related to water quality (Martellucci et al., 2021).
65 In this context, the present work integrates the state-of-the-art approach of *in situ* measurements (in 2014-2020, distributed by
66 Copernicus In Situ TAC) with the Copernicus biogeochemical reanalysis in the Mediterranean Sea at high resolution (Cossarini
67 et al., 2021), with the aim of characterizing the DO dynamics in the SAdr in the 1999-2021 time period. In particular, we aim
68 to assess DO inter-annual variability in an area (SAdr) sensitive to multiple drivers (e.g., atmospheric forcing, Mediterranean
69 circulation, and biological processes) and to evaluate the relative importance of the different drivers in this area.

70 **2 Data and methods**

71 In the present study the DO concentration in the SAdr area (Fig. 1a) was assessed by combining data from the Copernicus
72 reanalysis in the Mediterranean Sea (Prod1 in Table 1; Cossarini et al., 2021) in 1999-2021 and the Copernicus *in situ* dataset
73 (Prod2, <https://doi.org/10.13155/75807>), available for the period 2014-2020 (Figs. 1b-c). The temporal evolution of the
74 combined model-*in situ* DO concentration profile in 1999-2021 time period is shown in Fig. 1d.

75 In particular, we used the BGC-Argo float measurements of *in situ* DO to compute a bias correction to the daily DO
76 concentrations simulated by the biogeochemical reanalysis at $1/24^\circ$ horizontal resolution. In fact, the biogeochemical
77 reanalysis does not include BGC-Argo float DO assimilation and displays an average RMSD of 15 mmol m^{-3} for DO in the 0-
78 600 m depth layer with respect to the observations in the area (Cossarini et al., 2021, Teruzzi et al., 2021a-b). Quantile
79 Mapping, a technique largely used for climate simulations (e.g., Hopson and Webster, 2010; Themeßl et al., 2011;
80 Gudmundsson et al., 2012), was adopted to perform the reanalysis bias correction. The Quantile Mapping technique adjusts
81 the cumulative distribution of the data simulated for the past or future period by applying a transformation between the
82 quantiles of the simulated and observed data in the present. In our application, we adapted the code publicly provided by Beyer
83 et al. (2020) at <https://doi.org/10.17605/OSF.IO/8AXW9> and included available *in situ* data of daily DO (Fig. 1c) within a
84 representative area (Fig. 1b) of the southern Adriatic in the period 2014-2020, and DO reanalysis data for the same days of
85 measurements. The representative area was identified by applying a spatial cross-correlation analysis (Martellucci et al., 2021)
86 to the biogeochemical reanalysis centered on the SAdr pit and selecting the correlation threshold of 0.9 (Fig. 1b). Specifically,
87 we considered the cross-correlation between the surface data of DO, nitrate and chlorophyll concentrations in the central point
88 of the pit and those at each spatial grid point in the domain, to identify the area that displayed the same dynamics at the surface
89 from a phenomenological perspective. Further details on the Quantile Mapping bias correction are included in Appendix A.
90 We then applied the Empirical Orthogonal Function (EOF) analysis (e.g. Thomson and Emery, 2014) to the vertical profiles
91 in Fig. 1d to describe DO variability in the SAdr area in the period 1999-2021. The EOF analysis allows us to identify the

92 spatial patterns of variability (i.e., EOF vertical patterns), describe how they change in time by means of time series (i.e., EOF
93 time series), and associate the explained variance with each mode.

94 Finally, we performed a Pearson correlation analysis between the EOF time series in 1999-2021 and the following series of
95 forcing indexes (reported in Fig. 2) providing evidence of the mechanisms driving oxygen concentration and dynamics in the
96 area:

- 97 - heat fluxes in the SAdr as a proxy for thermal and mixing and stratification cycles (from Prod3; Fig. 2a);
- 98 - mixed layer depth in the SAdr as a proxy for both local vertical mixing and water residence times in the pit (Prod3; Fig. 2b);
- 99 - chlorophyll concentration at surface and in subsurface in the SAdr as a proxy for biological production in spring and late
100 spring-summer, respectively (Prod1; Fig. 2c-d);
- 101 - heat fluxes in the northern Adriatic Sea (NAAdr), as a proxy for dense water oxygen-rich formation in the NAAdr and its
102 transport into the pit (Prod3; Fig. 2e);
- 103 - Northern Ionian Gyre (NIG) vorticity derived from satellite altimetry, as a proxy of the inflow of Levantine waters and
104 Atlantic Water (AW) (Prod4 and Prod5; Fig. 2f).

105 In particular, the temporal phases of the NIG are defined as cyclonic and anticyclonic, respectively, when the vorticity field is
106 positive and negative, as highlighted by the de-seasonalized time series in Fig. 2f.

107 Mixed layer depth (computed in Prod3 considering the 0.03 kg m^{-3} density difference with respect to the near-surface value at
108 10 m depth) and the chlorophyll at surface and in subsurface (30-80 m, where the deep chlorophyll maximum is located) were
109 spatially averaged in the SAdr area (41.6° - 42.1° N; 17.6° - 18.1° E, to consider the whole volume of the pit); heat fluxes were
110 calculated in both the SAdr area and in the NAAdr area (44.5° - 45.5° N; 13° - 13.5° E), while current vorticity was computed in
111 the Northern Ionian Sea (37° - 39° N; 17° - 19.5° E).

112 In the correlation analysis, the time series of the heat fluxes in NAAdr Sea (Fig. 2e) has been temporally lagged by 2 months, as
113 an estimated mean time for the entrance in the SAdr pit of waters originated in the Northern Adriatic area (Vilibić et al., 2013;
114 Querin et al., 2016; Mihanović et al 2021). Moreover, we tested the significance of the correlation coefficients between EOF
115 and driver time series using a parametric t-test (with a reference significance level of 0.05).

116 **3 Results**

117 **3.1 Temporal scales of variability in connection with drivers**

118 Dissolved oxygen in the southern Adriatic area (Fig. 1a) shows in the subsurface layers an alternation between periods of
119 enrichment (in 2004-2006, 2010-2013, 2016-2017) and sharp declines that impacted the Oxygen Minimum Layer (OML),
120 located between 100 and 300 m. Low concentration values are observed also in the years between 1999 and 2003.

121 The EOF analysis was performed on the vertical profiles of the oxygen anomaly, derived by removing the mean profile in the
122 period 1999-2021, and then normalized dividing by their standard deviation.

123 The time series of the first four EOF modes, which explain up to 95% of the oxygen variability in the water column are shown
124 along with the corresponding vertical patterns in Figs. 3a,c,e,g and Figs. 3b,d,f,h, respectively.

125 The EOFs are interpreted considering the correlation of the EOF time series (Figs. 3a,c,e,g) with the time series of the forcing
126 indicators shown in Fig. 2 (see Table 2), with heat fluxes in the northern Adriatic Sea time-lagged by two months as the
127 estimated time of entry of the NAdr dense water in the SAdr pit.

128 The first mode (Figs. 3a-b), accounting for 48.9% of the explained variance, can be associated with the seasonal cycle of
129 oxygen concentration in the upper layers: its vertical pattern mainly affects the first levels (Fig. 3b), the corresponding time
130 series shows relative maximum values in spring (Fig. 3a) and it shows a statistically significant but moderate correlation
131 ($r=0.56$) with heat flux and a lower correlation with the subsurface chlorophyll concentration ($r=0.43$) in the SAdr area (first
132 column in Table 2).

133 The second and third modes (Figs. 3c-d and 3e-f, respectively), describing 19.7% and 17.7% of the variance respectively,
134 affected both the upper and deeper layers. Both modes display relative maximum values in summer, but they have different
135 correlation coefficients with the explanatory factors. The time series of the second mode (second column in Table 2) shows a
136 significant but low correlation with multiple drivers, exceeding 0.4 only for surface chlorophyll ($r=-0.41$) and waters from the
137 NAdr area ($r=0.48$). The time series of the third mode (third column, same Table) is moderately correlated with both surface
138 chlorophyll ($r=-0.61$) and NAdr waters ($r=0.68$ correlation), but also with heat fluxes in the area ($r=0.51$), and, to a lower
139 extent, with mixed layer depth ($r=-0.41$) and subsurface chlorophyll ($r=0.48$).

140 The fourth mode (Figs. 3g-h), that describes 8% of the variance, can be ascribed mainly to the vorticity of the NIG ($r=-0.37$,
141 last column in Table 2), which affects the oxygen concentration in the intermediate layer (100-500 m depth), filled by LIW,
142 and acts in the opposite direction in the upper and deeper layers (Fig. 3h).

143 Analysing the four modes in order of decreasing explained variance, we ascribe the seasonal variability connected with
144 solubility mainly to the first mode, whereas we associate the biological contribution to oxygen dynamics to multiple interacting
145 modes. In fact, the first mode explains the onset of the subsurface oxygen maximum (SOM) in spring, while the summer
146 dynamics of the SOM is partially related to the third mode. The second mode, whose time series is correlated with surface
147 chlorophyll evolution among other factors, can explain that part of the oxygen variability that is related to winter surface
148 productivity.

149 The SOM, evident in summer oxygen profiles in Figs. 1c-d at about 40 m depth, is a feature that has already been observed in
150 a great part of oligotrophic oceans (Riser and Johnson, 2008; Yasunaka et al., 2022) and of the Mediterranean Sea (e.g., Kress
151 and Herut, 2001; Copin-Montégut and Bégovic, 2002; Manca et al., 2004; Cossarini et al., 2021; Di Biagio et al., 2022) and it
152 represents an emerging property resulting from multiple interacting ecosystem processes (i.e., air-sea interactions, transport,
153 mixing and biological production and consumption) and is, indeed, captured by multiple modes.

154 The third mode, which also describes the high concentration values in the deep layers in the period 2005-2006 and 2012-2014,
155 is also moderately associated with a multi-annual signal of the inflow of deep denser and oxygenated water from the northern
156 Adriatic Sea ($r=0.68$, third column in Table 2; Querin et al., 2016). Finally, it is worth noting that an EOF analysis of detrended

157 DO time series (not shown) yields fairly similar results but with the third mode only weakly correlated with the forcing indexes
158 ($r < 0.4$). Indeed, we can conclude that the third mode captures a signal of long-term evolution of oxygen concentration
159 associated with changes in heat fluxes and chlorophyll concentration.

160 **3.2 The 2021 anomaly**

161 The year 2021 shows an overall negative anomaly in the oxygen concentration profile (Fig. 4b) compared to the 1999-2020
162 climatological profiles (Fig. 4a). In particular, the anomaly affects a layer that thinned during the year, moving from 0-600 m
163 depth in winter-early spring season to 30-400 m in late spring-summer and 0-80 m in fall. The (absolute) maximum values
164 correspond to 25-30 mmol m⁻³ at the surface in spring and at the SOM depth in summer.

165 We verified that, among the EOF modes, the negative anomaly of the first mode is the main contributor to the 2021 negative
166 oxygen anomaly (not shown). The time series of the first mode (Fig. 3a) is actually negative from 2019 and corresponds to
167 the negative anomaly of only one of its drivers (Table 2), i.e. subsurface chlorophyll (Fig. 2d), and not heat fluxes (Fig. 2a).
168 In particular, we estimated a mean negative anomaly approximately equal to 6% with respect to the climatological mean (1999-
169 2020) for subsurface chlorophyll in 2021.

170 One of the causes of the decrease in total oxygen concentration in the SAdr could be due to the exceptional salinization
171 observed in the SAdr since 2017 (Mihanović et al., 2021, Menna et al., 2022b). This increase was related to the inflow of new,
172 warmer and noticeably saltier water masses from the northeastern Ionian Sea (Mihanović et al., 2021, Menna et al., 2022b).
173 The inflow of saltier and warmer water masses is also evident by observing the temporal evolution of these parameters through
174 the Strait of Otranto (Fig. B1). In particular, in the upper layer (0-150 m) both temperature and salinity show an overall positive
175 trend throughout the period 1999-2021, whereas the decrease observed in 2006-2011 and 2017-2018 can be associated with
176 the inflow of less saline AW, triggered by the anticyclonic circulation of the NIG (Fig. 2f). In the intermediate layer (150-600
177 m), salinity shows a positive trend in 1999-2021, while no clear trend is observed for temperature. Moreover, a sharp increase
178 in salinity (~ 0.1) is observed in 2019. This increase occurred after the NIG inversion from anticyclonic to cyclonic (Fig. 2f),
179 resulting in a further increase in salinity due to both the decrease in AW advection and the increase in LIW inflow.

180 **4 Conclusions**

181 Merging the Copernicus biogeochemical reanalysis in the Mediterranean Sea with *in situ* TAC data of biogeochemical Argo
182 floats allowed us to characterize the interannual variability of dissolved oxygen in the Southern Adriatic Sea in the 1999-2021
183 time period and the 2021 anomaly with respect to the mean over 1999-2020. This study enriches our knowledge of the dissolved
184 oxygen state and long-term dynamics in the area, by proposing a seamless time and space perspective that is complementary
185 to previous climatologies and data aggregation information (e.g. Lipizer et al., 2014) and adding an explanatory framework
186 for the driving mechanisms in the marine environment.

187 The EOF statistical analysis that we conducted on the vertical oxygen profiles yielded two key results. First, in contrast with
188 a climatological view, the analysis was able to capture most of the inter-annual oxygen variability associated with variability
189 of the main drivers (i.e., heat fluxes affecting solubility; biological productivity; vertical mixing). We do not detect a clear
190 deoxygenation trend in the subsurface layer, while the multiannual variability is characterised by an alternation of enrichment
191 and reduction phases, whose dominant correlations with the drivers for each EOF time series are in the (absolute) range 0.40-
192 0.70. The possibility to observe such cyclic signals is enhanced by the relatively small volume and short residence time of the
193 SAdr pit waters (Querin et al., 2016) with respect to other Mediterranean areas (Coppola et al., 2018). This feature makes the
194 SAdr a potential efficient probe to detect a rapid response to changes in its meteo-marine drivers, i.e., circulation and
195 atmospheric patterns.

196 Indeed, as our second result, the variability that is not explained by the EOF decomposition appears to be connected with a
197 possible regime shift, associated with the entrance of new water masses, warmer, markedly saltier and less oxygenated, that
198 were not previously observed in the analyzed time period.

199 The exceptional increase in salinity occurring after 2019 has been already documented (Mihanović et al., 2021; Menna et al.,
200 2022b) and also observed north of the SAdr pit. Further monitoring of such anomalously high salinity values and assessment
201 of their potential impact on the marine food web is of great importance, as picoplankton groups are sensitive to this
202 environmental variable (Mella-Flores et al., 2011) and changes in biomass and production due to salinity have already been
203 observed in previous studies in the Adriatic Sea (Beg Paklar et al., 2020; Mauri et al., 2021). Moreover, if such a strong
204 negative oxygen anomaly as observed in 2021 were to persist, it could have direct impacts on local marine organisms, as well
205 as on the cycling of dissolved chemical elements (Conley et al., 2009) potentially altering the energy flux towards the higher
206 trophic levels (Ekau et al., 2010). The importance of the relationship between dissolved oxygen and the catch distribution of
207 some marine species has already been proved in the Adriatic Sea (Chiarini et al., 2022).

208 By integrating model and *in situ* data, our study demonstrates the importance of following up the oxygen content in a seamless
209 spatial and temporal way, as it is a fundamental indicator of good environmental status (GES, Oesterwind et al., 2016) and a
210 factor that significantly affects fishing activities and economy.

211

212 **Appendix A: Quantile Mapping bias correction of DO concentration profiles**

213 Figures A1 and A2 show the modelled DO concentration profiles and histogram distributions before and after the Quantile
214 Mapping bias correction, respectively, conducted by using the BGC-Argo float measurements available in 2014-2020 (Fig.
215 1c). The Quantile Mapping, better than other methods (i.e. Additive Delta Change, Multiplicative Delta Change and Variance
216 Scaling; results not shown), acted on the profiles by modifying the values of the concentrations (as indicated by the different
217 colorbars in Figs. A1a and A1b) but, at the same time, maintaining the main dynamics observed before the correction: mixing
218 and stratification at the surface during the year, subsurface oxygen maximum onset in spring and development in summer, and
219 interannual variability related to the mixed layer depth dynamics in the intermediate layers. The distributions of the values of
220 the model output before and after the Quantile Mapping bias correction and the values from BGC-Argo floats are displayed in

221 Fig. A2. The correction actually changed the modelled values (Fig. A2a) to reproduce the shape of the distribution of the
222 observations (Fig. A2c). In particular, after the correction (Fig. A2b) the modelled data show higher variability and a more
223 skewed distribution toward the higher values, similarly to the observations.

224

225 **Appendix B: Time series of surface and intermediate temperature and salinity at the Otranto Strait**

226

227 **Data availability**

228 Publicly available datasets were analyzed in this study. Modelling and *in situ* data can be found at the Copernicus Marine
229 Service, with references and DOIs indicated in the Table 1 of the manuscript.

230

231 **Author contribution**

232 VDB and GC conceived the idea. VDB, RM and MM conducted the analysis. VDB, RM and GC wrote the first draft, with
233 contributions from the other co-authors. All the authors discussed and reviewed the submitted manuscript.

234

235 **Competing interests**

236 The authors declare that they have no conflict of interest.

237

238 **Acknowledgements**

239 This study has been conducted using EU Copernicus Marine Service Information.

240 **Financial support**

241 This study has been partly funded by the Mediterranean Copernicus Monitoring and Forecast Center (contract LOT
242 REFERENCE: 21002L5-COP-MFC MED-5500 issued by Mercator Ocean) within the framework of Marine Copernicus
243 Service.

244 **References**

245 Batistić, M., Garić, R., & Molinero, J. C. (2014). Interannual variations in Adriatic Sea zooplankton mirror shifts in circulation
246 regimes in the Ionian Sea. *Climate research*, 61(3), 231-240, 2014.

247

248 Beg Paklar, G., Vilibić, I., Grbec, B., Matić, F., Mihanović, H., Džoić, T., et al.: Record-breaking salinities in the middle
249 Adriatic during summer 2017 and concurrent changes in the microbial food web. *Prog. Oceanogr.* 185:102345. doi:
250 10.1016/j.pocean.2020.102345, 2020.

251

252 Beyer, R., Krapp, M., and Manica, A.: An empirical evaluation of bias correction methods for palaeoclimate simulations, *Clim.*
253 *Past*, 16, 1493–1508, <https://doi.org/10.5194/cp-16-1493-2020>, 2020.

254

255 Breitburg, D., Levin, L. A., Oschlies, A., Grégoire, M., Chavez, F. P., Conley, D. J., ... & Zhang, J: Declining oxygen in the
256 global ocean and coastal waters. *Science*, 359(6371), eaam7240, 2018.

257

258 Chiarini, M., Guicciardi, S., Angelini, S., Tuck, I. D., Grilli, F., Penna, P., ... & Martinelli, M.: Accounting for environmental
259 and fishery management factors when standardizing CPUE data from a scientific survey: A case study for *Nephrops norvegicus*
260 in the Pomo Pits area (Central Adriatic Sea). *PloS one*, 17(7), e0270703, 2022.

261

262 Civitarese, G., Gačić, M., Lipizer, M., & Eusebi Borzelli, G. L.: On the impact of the Bimodal Oscillating System (BiOS) on
263 the biogeochemistry and biology of the Adriatic and Ionian Seas (Eastern Mediterranean). *Biogeosciences*, 7(12), 3987-3997.
264 <https://doi.org/10.5194/bg-7-3987-2010>, 2010.

265

266 Conley, D. J., Björck, S., Bonsdorff, E., Carstensen, J., Destouni, G., Gustafsson, B. G., ... & Zillén, L.: Hypoxia-related
267 processes in the Baltic Sea. *Environmental Science & Technology*, 43(10), 3412-3420, 2009.

268

269 Copin-Montégut, C. and Bégovic, M.: Distributions of carbonate properties and oxygen along the water column (0-2000 m)
270 in the central part of the NW Mediterranean Sea (dyfamed site): Influence of winter vertical mixing on air-sea CO₂ and O₂
271 exchanges, *Deep. Res. Part II Top. Stud. Oceanogr.*, 49(11), 2049–2066, doi:10.1016/S0967-0645(02)00027-9, 2002.

272

273 Coppola, L., Legendre, L., Lefevre, D., Prieur, L., Taillandier, V. and Diamond Riquier, E.: Seasonal and inter-annual
274 variations of dissolved oxygen in the northwestern Mediterranean Sea (DYFAMED site), *Prog. Oceanogr.*, 162(January), 187–
275 201, doi:10.1016/j.pocean.2018.03.001, 2018.

276

277 Cossarini, G., Feudale, L., Teruzzi, A., Bolzon, G., Coidessa, G., Solidoro, C., Di Biagio, V., Amadio, C., Lazzari, P., Brosich,
278 A. and Salon, S.: High-resolution reanalysis of the Mediterranean Sea biogeochemistry (1999-2019). *Frontiers in Marine*
279 *Science*, 1537, <https://doi.org/10.3389/fmars.2021.741486>, 2021.

280

281 Cushman-Roisin, B., Gacic, M., Poulain, P. M., & Artegiani, A. (Eds.): *Physical oceanography of the Adriatic Sea: past,*
282 *present and future.* Springer Science & Business Media, 2013.

283

284 Di Biagio, V., Salon, S., Feudale, L., and Cossarini, G.: Subsurface oxygen maximum in oligotrophic marine ecosystems:
285 mapping the interaction between physical and biogeochemical processes, *Biogeosciences* 19, 5553–5574,
286 <https://doi.org/10.5194/bg-19-5553-2022>, 2022.

287

288 Ekau, W., Auel, H., Pörtner, H. O., & Gilbert, D.: Impacts of hypoxia on the structure and processes in pelagic communities
289 (zooplankton, macro-invertebrates and fish). *Biogeosciences*, 7(5), 1669-1699, 2013.

290

291 Escudier, R., Clementi, E., Omar, M., Cipollone, A., Pistoia, J., Aydogdu, A., Drudi, M., Grandi, A., Lyubartsev, V., Lecci,
292 R., Cretí, S., Masina, S., Coppini, G., & Pinardi, N. Mediterranean Sea Physical Reanalysis (CMEMS MED-Currents) (Version
293 1) [Data set](#). Copernicus Monitoring Environment Marine Service
294 (CMEMS). https://doi.org/10.25423/CMCC/MEDSEA_MULTIYEAR_PHY_006_004_E3R1, 2020.

295

296 Escudier R., Clementi E., Cipollone A., Pistoia J., Drudi M., Grandi A., Lyubartsev V., Lecci R., Aydogdu A., Delrosso D.,
297 Omar M., Masina S., Coppini G. and Pinardi N.: A High Resolution Reanalysis for the Mediterranean Sea. *Front. Earth Sci.*
298 9:702285. <https://doi.org/10.3389/feart.2021.702285>, 2021.

299

300 Gačić, M., Civitarese, G., Miserocchi, S., Cardin, V., Crise, A., & Mauri, E.: The open-ocean convection in the Southern
301 Adriatic: a controlling mechanism of the spring phytoplankton bloom. *Continental Shelf Research*, 22(14), 1897-1908, 2002.

302

303 Gačić, M.; Borzelli, G.E.; Civitarese, G.; Cardin, V.; Yari, S.; Can internal processes sustain reversals of the ocean upper
304 circulation? The Ionian Sea example. *Geophys. Res. Lett.*, 37 (9) :L09608, DOI:10.1029/2009JC005749, 2010.

305

306 Gačić, M.; Civitarese, G.; Eusebi Borzelli, G.L.; Kovačević, V.; Poulain, P.M.; Theocharis, A.; Menna, M.; Catucci, A.;
307 Zarokanellos, N.; On the relationship between the decadal oscillations of the northern Ionian Sea and the salinity distributions
308 in the eastern Mediterranean.; *J. Geophys. Res. Oceans*, 116, C12, <https://doi.org/10.1029/2011JC007280>, 2011.

309

310 Gačić, M.; Ursella, L.; Kovačević, V.; Menna, M.; Malačić, V.; Bensi, M.; Negretti, M.E.; Cardin, V.; Orlić, M.; Sommeria,
311 J.; Barreto, R.V.; Viboud, S.; Valran, T.; Petelin, B.; Siena, G.; Rubino, A.; Impact of dense-water flow over a sloping bottom
312 on open-sea circulation: laboratory experiments and an Ionian Sea (Mediterranean) example. *Ocean Sci.*, 17, 975–996,
313 <https://doi.org/10.5194/os-17-975-2021>, 2021.

314

315 Garcia-Soto, C., Cheng, L., Caesar, L., Schmidtko, S., Jewett, E. B., Cheripka, A., Rigor I., Caballero A., Chiba S., Báez J.
316 C., Zielinski T. and Abraham, J. P.: An overview of ocean climate change indicators: Sea surface temperature, ocean heat
317 content, ocean pH, dissolved oxygen concentration, arctic sea ice extent, thickness and volume, sea level and strength of the

318 AMOC (Atlantic Meridional Overturning Circulation). *Frontiers in Marine Science*.
319 <https://www.frontiersin.org/article/10.3389/fmars.2021.642372>, 2021.
320
321 Gudmundsson, L., Bremnes, J. B., Haugen, J. E., & Engen-Skaugen, T.: Downscaling RCM precipitation to the station scale
322 using statistical transformations—a comparison of methods. *Hydrology and Earth System Sciences*, 16(9), 3383-3390, 2012.
323
324 Hersbach, H., Bell, B., Berrisford, P., Biavati, G., Horányi, A., Muñoz Sabater, J., Nicolas, J., Peubey, C., Radu, R., Rozum,
325 I., Schepers, D., Simmons, A., Soci, C., Dee, D., Thépaut, J-N.: ERA5 hourly data on single levels from 1959 to present.
326 Copernicus Climate Change Service (C3S) Climate Data Store (CDS). (Accessed on 6-3-2023), 10.24381/cds.adbb2d47, 2018.
327
328 Hopson, T. M., & Webster, P. J.: A 1–10-day ensemble forecasting scheme for the major river basins of Bangladesh:
329 Forecasting severe floods of 2003–07. *Journal of Hydrometeorology*, 11(3), 618-641, 2010.
330
331 Jakob Themeßl, M., Gobiet, A. and Leuprecht, A.: Empirical-statistical downscaling and error correction of daily precipitation
332 from regional climate models. *Int. J. Climatol.*, 31: 1530-1544. <https://doi.org/10.1002/joc.2168>, 2011.
333
334 Keeling, R. F., & Garcia, H. E.: The change in oceanic O₂ inventory associated with recent global warming. *Proceedings of*
335 *the National Academy of Sciences*, 99(12), 7848-7853, 2002.
336
337 Kokkini Z., Mauri E., Gerin R., Poulain P.-M., Simoncelli S., Notarstefano G.: On the salinity structure in the South Adriatic
338 as derived from float and glider observations in 2013–2016. *Deep-Sea Research Part II* 11 pp, 2019.
339
340 Kokkini Z., Notarstefano G., Poulain P.-M., Mauri E., Gerin R., Simoncelli S. (2018). In Von Schuckmann et al.: Unusual
341 salinity pattern in the South Adriatic Sea. Copernicus Marine Service Ocean State Report 2018-09-08 - *Journal of Operational*
342 *Oceanography*, 11:sup1, S1-S142, 2018.
343
344 Kress, N., & Herut, B.: Spatial and seasonal evolution of dissolved oxygen and nutrients in the Southern Levantine Basin
345 (Eastern Mediterranean Sea): chemical characterization of the water masses and inferences on the N: P ratios. *Deep Sea*
346 *Research Part I: Oceanographic Research Papers*, 48(11), 2347-2372, 2001.
347
348 Kwiatkowski, L., Torres, O., Bopp, L., Aumont, O., Chamberlain, M., Christian, J. R., ... & Ziehn, T.: Twenty-first century
349 ocean warming, acidification, deoxygenation, and upper-ocean nutrient and primary production decline from CMIP6 model
350 projections. *Biogeosciences*, 17(13), 3439-3470. <https://doi.org/10.5194/bg-17-3439-2020>, 2020.
351

352 Lipizer, M., Partescano, E., Rabitti, A., Giorgetti, A., & Crise, A.: Qualified temperature, salinity and dissolved oxygen
353 climatologies in a changing Adriatic Sea. *Ocean Science*, 10(5), 771-797. <https://doi.org/10.5194/os-10-771-2014>, 2014.
354

355 Malanotte-Rizzoli, P., Manca, B. B., d'Alcala, M. R., Theocharis, A., Brenner, S., Budillon, G., & Ozsoy, E. The Eastern
356 Mediterranean in the 80s and in the 90s: the big transition in the intermediate and deep circulations. *Dynamics of Atmospheres*
357 *and Oceans*, 29(2-4), 365-395, 1999.
358

359 Manca, B., Burca, M., Giorgetti, A., Coatanoan, C., Garcia, M. J., & Iona, A.: Physical and biochemical averaged vertical
360 profiles in the Mediterranean regions: an important tool to trace the climatology of water masses and to validate incoming data
361 from operational oceanography. *Journal of Marine Systems*, 48(1-4), 83-116, 2004.
362

363 Manca, B., Ibello, V., Pacciaroni, M., Scarazzato, P., & Giorgetti, A. Ventilation of deep waters in the Adriatic and Ionian
364 Seas following changes in thermohaline circulation of the Eastern Mediterranean. *Climate Research*, 31(2-3), 239-256, 2006.
365

366 Martellucci, R., Salon, S., Cossarini, G., Piermattei, V., & Marcelli, M.: Coastal phytoplankton bloom dynamics in the
367 Tyrrhenian Sea: Advantage of integrating in situ observations, large-scale analysis and forecast systems. *Journal of Marine*
368 *Systems*, 218, 103528, 2021.
369

370 Matear, R. J., Hirst, A. C., & McNeil, B. I.: Changes in dissolved oxygen in the Southern Ocean with climate
371 change. *Geochemistry, Geophysics, Geosystems*, 1(11), 2000.
372

373 Mauri E, Menna M, Garić R, Batistić M, Libralato S, Notarstefano G, Martellucci R, Gerin R, Pirro A, Hure M, Poulain P-M.
374 Recent changes of the salinity distribution and zooplankton community in the South Adriatic Pit, *Journal of Operational*
375 *Oceanography*, Copernicus Marine Service Ocean State Report, Issue 5. 14 (sup1), pp.1-185,
376 <https://doi.org/10.1080/1755876X.2021.1946240>, 2021.
377

378 Mavropoulou, A. M., Vervatis, V. and Sofianos, S.: Dissolved oxygen variability in the Mediterranean Sea, *J. Mar. Syst.*,
379 208(March), doi:10.1016/j.jmarsys.2020.103348, 2020.
380

381 Mella-Flores, D., Mazard, S., Humily, F., Partensky, F., Mahe, F., Bariat, L., et al.: Is the distribution of *Prochlorococcus* and
382 *Synechococcus* ecotypes in the Mediterranean Sea affected by global warming? *Biogeosciences* 8, 2785–2804. doi:
383 10.5194/bg-8-2785-2011, 2011.
384

385 Menna, M.; Reyes-Suarez, N.C.; Civitarese, G.; Gačić, M.; Poulain, P.-M.; Rubino, A.; Decadal variations of circulation in
386 the Central Mediterranean and its interactions with the mesoscale gyres. *Deep Sea Res. Part II Top. Stud. Oceanogr.*, 164, 14-
387 24, <https://doi.org/10.1016/j.dsr2.2019.02.004>, 2019.

388

389 Menna M., Gačić M., Martellucci R., Notarstefano G., Fedele G., Mauri E., Gerin R., Poulain P.-M.: Climatic, decadal and
390 interannual variability in the upper layer of the Mediterranean Sea using remotely sensed and in-situ data. *Remote sensing*,
391 14, 1322. <https://doi.org/10.3390/rs14061322>, 2022a.

392

393 Menna, M., Martellucci, R., Notarstefano, G., Mauri, E., Gerin, R., Pacciaroni, M., Bussani, A., Pirro, A., Poulain, P.-M. :
394 Record-breaking high salinity in the South Adriatic Pit in 2020, Copernicus Marine Service Ocean State Report 6 - Journal of
395 Operational Oceanography, 2022b.

396

397 Mihanović, H., Vilibić, I., Šepić, J., Matić, F., Ljubešić, Z., Mauri, E., ... & Poulain, P. M.: Observation, Preconditioning and
398 Recurrence of Exceptionally High Salinities in the Adriatic Sea. *Frontiers in Marine Science*, 8, 834.
399 <https://doi.org/10.3389/fmars.2021.672210>, 2021.

400

401 Oesterwind, Daniel, Andrea Rau, and Anastasija Zaiko: Drivers and pressures—untangling the terms commonly used in marine
402 science and policy. *Journal of environmental management* 181, 8-15, 2016.

403

404 Oeschies, A., Schulz, K. G., Riebesell, U., & Schmittner, A.: Simulated 21st century's increase in oceanic suboxia by CO2-
405 enhanced biotic carbon export. *Global Biogeochemical Cycles*, 22(4), 2008.

406

407 Oeschies, A., Brandt, P., Stramma, L., & Schmidtko, S.: Drivers and mechanisms of ocean deoxygenation. *Nature Geoscience*,
408 11(7), 467-473, 2018.

409

410 Querin, S., M. Bensi, V. Cardin, C. Solidoro, S. Bacer, L. Mariotti, F. Stel, and V. Malac'ic': Saw-tooth modulation of the
411 deep-water thermohaline properties in the southern Adriatic Sea, *J. Geophys. Res. Oceans*, 121, 4585–4600,
412 <https://doi.org/10.1002/2015JC011522>, 2016.

413

414 Pirro, A., Mauri, E., Gerin, R., Martellucci, R., Zuppelli, P., & Poulain, P. M.: New insights on the formation and breaking
415 mechanism of convective cyclonic cones in the South Adriatic Pit during winter 2018. *Journal of Physical Oceanography*,
416 2022.

417

418 Pitcher, G. C., Aguirre-Velarde, A., Breitburg, D., Cardich, J., Carstensen, J., Conley, D. J., ... & Zhu, Z. Y.: System controls
419 of coastal and open ocean oxygen depletion. *Progress in Oceanography*, 197, 102613, 2021.

420

421 Pörtner, H. O., Roberts, D. C., Masson-Delmotte, V., Zhai, P., Tignor, M., Poloczanska, E., & Weyer, N. M. The ocean and
422 cryosphere in a changing climate. IPCC Special Report on the Ocean and Cryosphere in a Changing Climate. Cambridge
423 University Press, Cambridge, UK and New York, NY, USA, 755 pp., <https://doi.org/10.1017/9781009157964>, 2019.

424

425 Reale, M., Cossarini, G., Lazzari, P., Lovato, T., Bolzon, G., Masina, S., Solidoro, C., and Salon, S.: Acidification,
426 deoxygenation, nutrient and biomasses decline in a warming Mediterranean Sea, *Biogeosciences* 19, 4035–4065,
427 <https://doi.org/10.5194/bg-19-4035-2022>, 2022.

428

429 Riser, S. C. and Johnson, K. S.: Net production of oxygen in the subtropical ocean, *Nature*, 451(7176), 323–325,
430 doi:10.1038/nature06441, 2008.

431

432 Rubino, A.; Gačić, M.; Bensi, M.; Kovačević, V.; Malačić, V.; Menna, M.; Negretti, M.E.; Sommeria, J.; Zanchettin, D.;
433 Barreto, R.V.; et al. Experimental evidence of long-term oceanic circulation reversals without wind influence in the North
434 Ionian Sea. *Sci. Rep.*, 10, 1905, 10.1038/s41598-020-57862-6, 2020.

435

436 Teruzzi, A., Di Biagio, V., Feudale, L., Bolzon, G., Lazzari, P., Salon, S., Coidessa, G., & Cossarini, G. Mediterranean Sea
437 Biogeochemical Reanalysis (CMEMS MED-Biogeochemistry, MedBFM3 system) (Version 1) [Data set](#). Copernicus
438 Monitoring Environment Marine Service
439 (CMEMS). https://doi.org/10.25423/CMCC/MEDSEA_MULTIYEAR_BGC_006_008_MEDBFM3, 2021a.

440

441 Teruzzi, A., Feudale, L., Bolzon, G., Lazzari, P., Salon, S., Di Biagio, V., Coidessa, G., & Cossarini, G. Mediterranean Sea
442 Biogeochemical Reanalysis INTERIM (CMEMS MED-Biogeochemistry, MedBFM3i system) (Version 1) Data set.
443 Copernicus Monitoring Environment Marine Service
444 (CMEMS) https://doi.org/10.25423/CMCC/MEDSEA_MULTIYEAR_BGC_006_008_MEDBFM3I (accessed March 6,
445 2023), 2021b.

446 Themeßl J., M., Gobiet, A. and Leuprecht, A. Empirical-statistical downscaling and error correction of daily precipitation from
447 regional climate models. *Int. J. Climatol.*, 31: 1530-1544. <https://doi.org/10.1002/joc.2168>, 2011.

448

449 Stramma, L., Schmidtko, S., Levin, L. A., & Johnson, G. C.: Ocean oxygen minima expansions and their biological impacts.
450 *Deep Sea Research Part I: Oceanographic Research Papers*, 57(4), 587-595, 2010.

451

452 Thomson, Richard E., and William J. Emery. Data analysis methods in physical oceanography. Newnes, 2014.

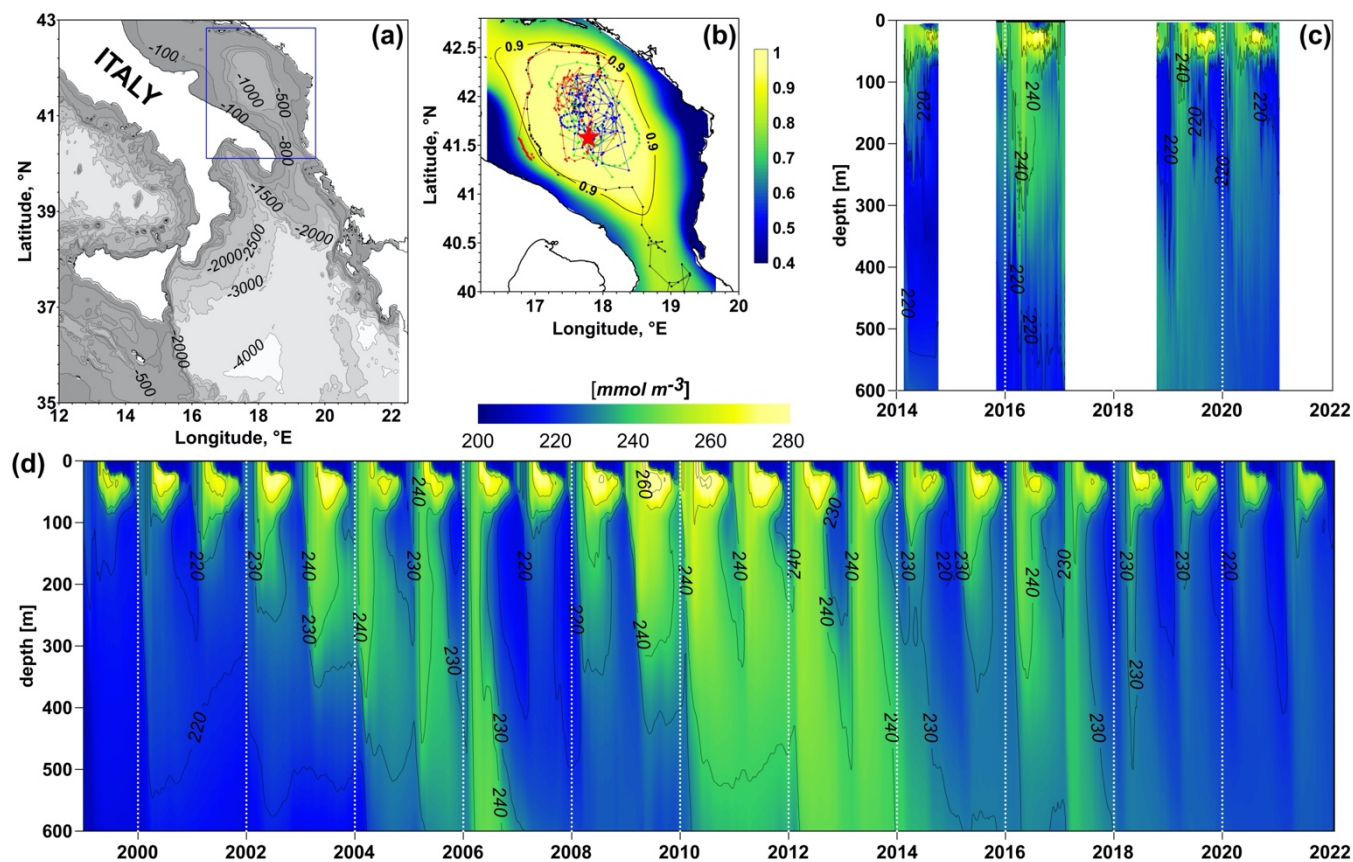
453

454 Vilibić, I., and Mihanović, H.: Observing the bottom density current over a shelf using an Argo profiling float, Geophys. Res.
455 Lett., 40, 910–915, doi:[10.1002/grl.50215](https://doi.org/10.1002/grl.50215), 2013.

456

457 Yasunaka, S., Ono, T., Sasaoka, K., and Sato, K.: Global distribution and variability of subsurface
458 chlorophyll a concentrations, Ocean Sci., 18, 255–268, <https://doi.org/10.5194/os-18-255-2022>, 2022.

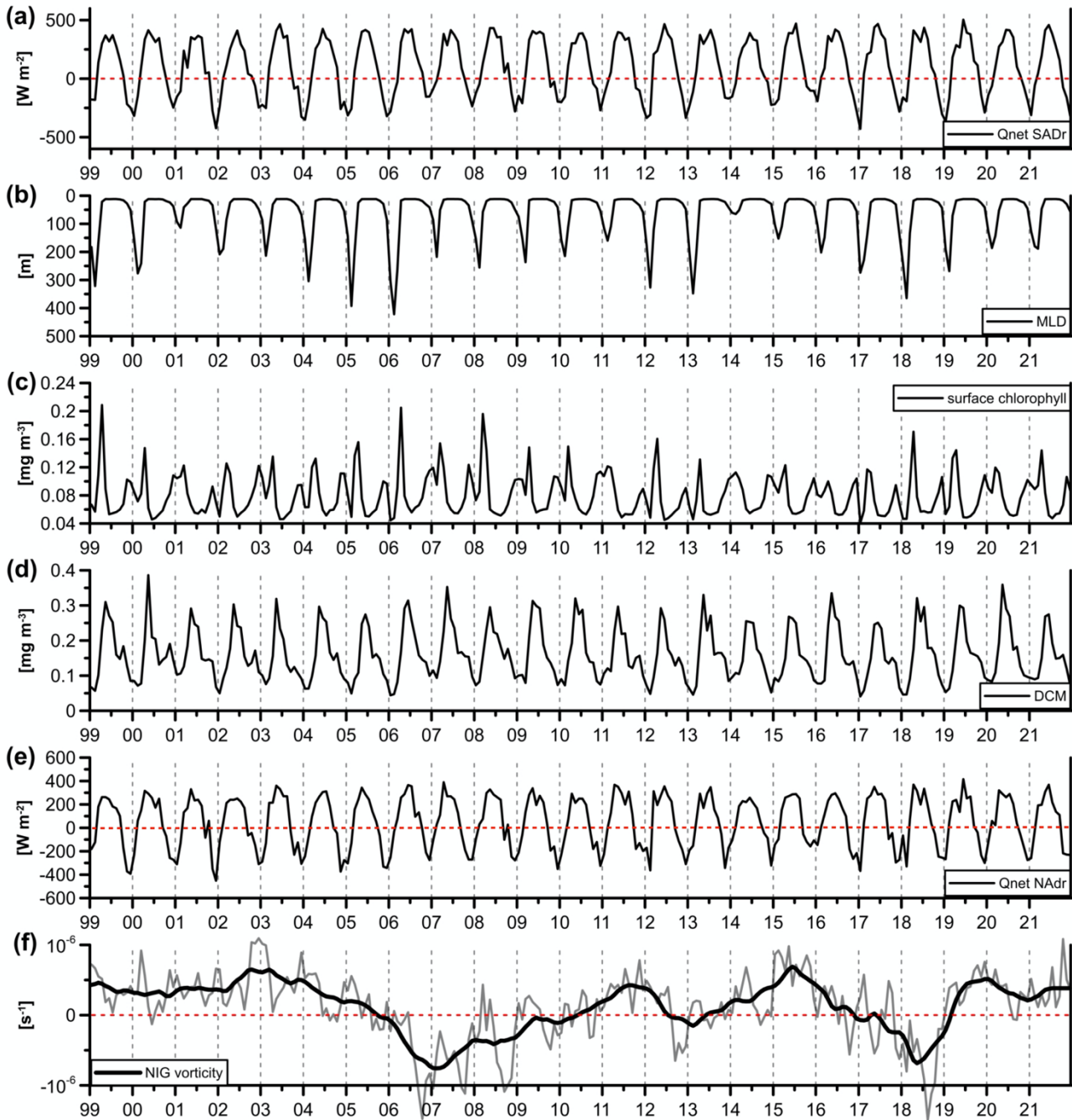
459



460

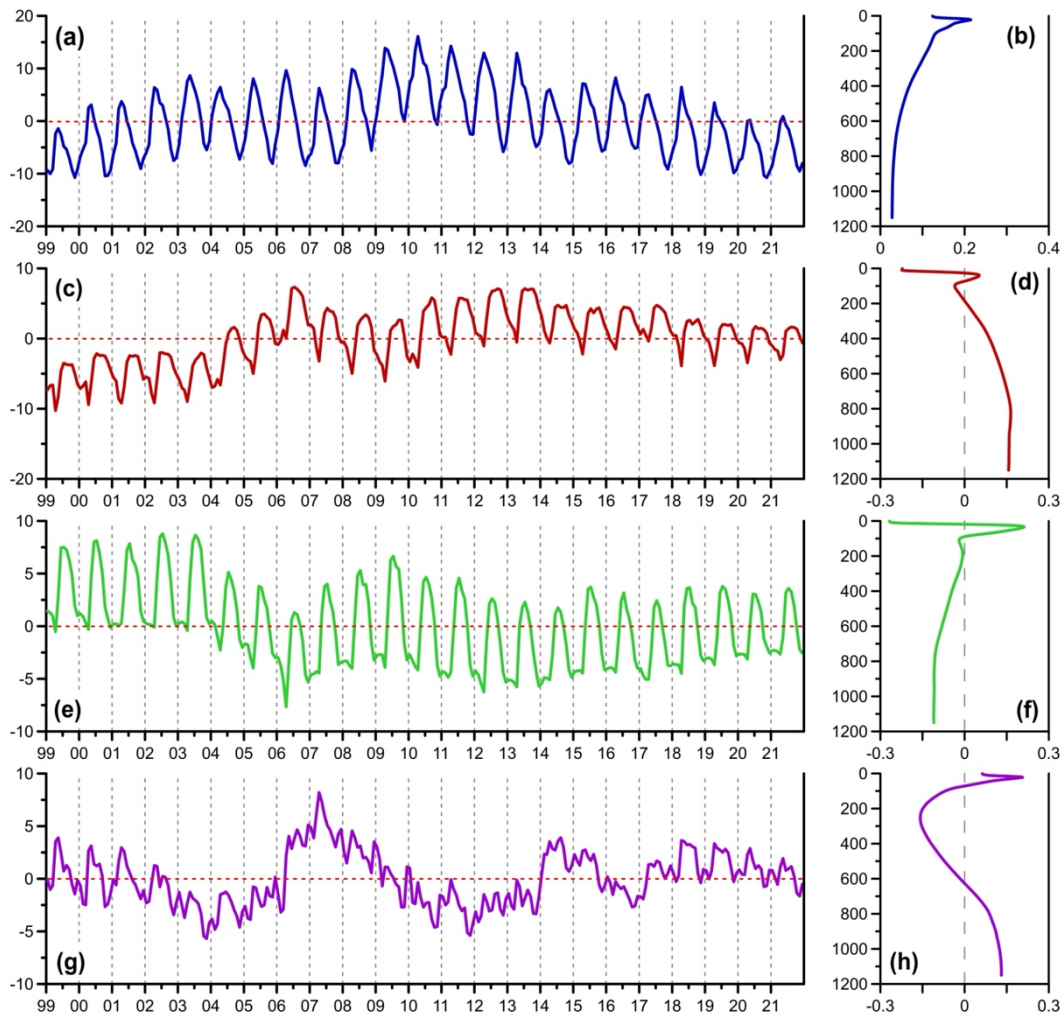
461 **Figure 1:** (a) Southern Adriatic area (blue square) within Mediterranean Sea; (b) Cross-correlation map of surface oxygen, nitrate
462 and chlorophyll concentration provided by Copernicus biogeochemical reanalysis (Prod1, Table 1) in the southern Adriatic area
463 with respect to the central point of the pit indicated by the red star; the black contour line delimits the area with cross-correlation
464 equal or higher than 0.9; dashed lines indicate the trajectories of BGC-Argo floats (In Situ TAC data, Prod2) passing the area. (c)
465 Hovmöller diagrams of the dissolved oxygen concentration from In Situ TAC data (Prod2) within the 0.9 cross-correlation area
466 (panel (b)). Data have been interpolated for readability of the plot. (d) Hovmöller diagrams of dissolved oxygen concentration from
467 Copernicus biogeochemical reanalysis (Prod1), spatially averaged within the area of cross-correlation equal to 0.9 (panel (a)) in
468 1999–2021 time period, after the bias correction procedure based on In Situ TAC data (Prod2).

469



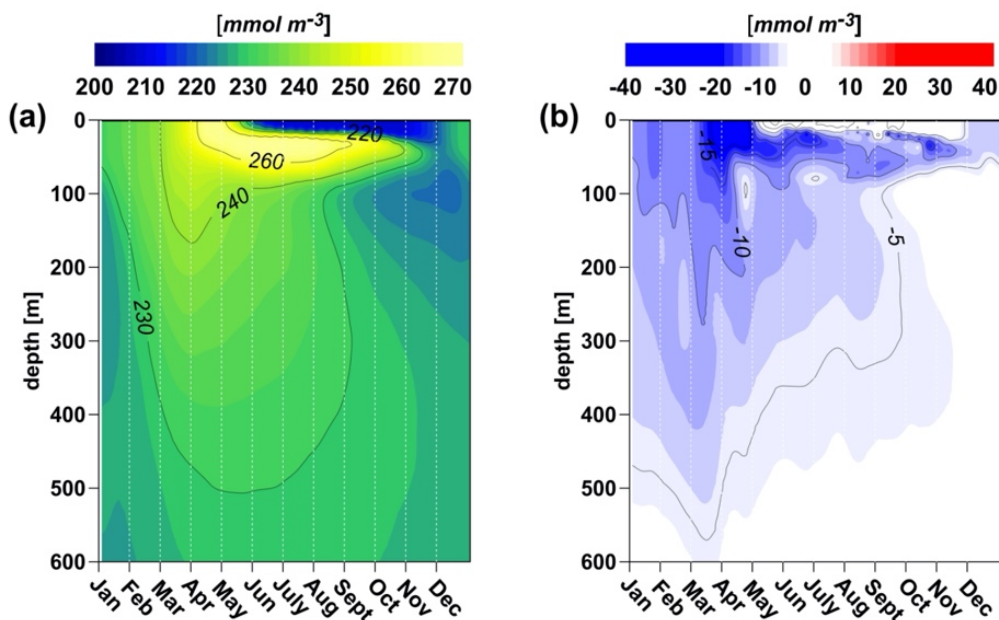
470

471 **Figure 2: Time series of the main forcing in the 1999-2021 time period: (a) net heat fluxes in SAdr (Prod6 in Table 1), (b) mixed**
 472 **layer depth (Prod3), (c) surface chlorophyll concentration (Prod1), (d) subsurface chlorophyll concentration (30-80 m layer in which**
 473 **deep chlorophyll maximum (DCM) is located, Prod1), (e) net heat fluxes in NAdr (Prod6), (f) NIG current vorticity (gray line) and**
 474 **de-seasonalized time series as obtained by applying a low-pass filter of 13 months) (Prod4 and Prod5).**



475

476 **Figure 3: EOF time series (a, c, e, g) and vertical patterns (b, d, f, h) of the first four modes computed on the bias-corrected dissolved**
 477 **oxygen concentration in the southern Adriatic area shown in Fig. 1d. The explained variances of the four modes are: 48.9%, 19.7%,**
 478 **17.7% and 8.4%.**



479

480

481 Figure 4: Hovmöller diagrams of: mean over 1999-2020 of daily oxygen concentration computed from Copernicus biogeochemical
 482 reanalysis (Prod1, Table 1) after the bias correction procedure based on In Situ TAC data (Prod2) (a) and anomaly in 2021 with
 483 respect to the 1999-2020 period (b).

484

485

Ref. no.	Product name & type	Documentation
1	Copernicus Marine MEDSEA_MULTIYEAR_BGC_006_008 Mediterranean Sea Biogeochemistry Reanalysis	Cossarini et al., (2021) Dataset: Teruzzi et al., (2021a, 2021b) https://doi.org/10.25423/CMCC/MEDSEA_MULTIYEAR_BGC_006_008_MEDBFM3 (Accessed on 6-3-2023) https://doi.org/10.25423/CMCC/MEDSEA_MULTIYEAR_BGC_006_008_MEDBFM3I (Accessed on 6-3-2023)

2	Copernicus Marine INSITU_MED_NRT_OBSERVATIONS_013_035 Mediterranean Sea-In-Situ Near Real Time Observations	Copernicus Marine in situ TAC (2021). Copernicus Marine In Situ TAC quality information document for Near Real Time In Situ products (QUID and SQO). https://doi.org/10.13155/75807 (Accessed on 6-3-2023)
3	Copernicus Marine MEDSEA_MULTIYEAR_PHY_006_004 Mediterranean Sea Physics reanalysis	Escudier et al., (2021) Dataset: Escudier et al., (2020) https://doi.org/10.25423/CMCC/MEDSEA_MULTIYEAR_PHY_006_004_E3R1 (Accessed on 6-3-2023)
4	Copernicus Marine SEALEVEL_EUR_PHY_L4_MY_008_068 European Seas Gridded L 4 Sea Surface Heights And Derived Variables Reprocessed 1993 Ongoing	https://doi.org/10.48670/moi-00141 (Accessed on 6-3-2023)
5	Copernicus Marine SEALEVEL_EUR_PHY_L4_NRT_OBSERVATIONS_008_060 European Seas Gridded L 4 Sea Surface Heights And Derived Variables Nrt	https://doi.org/10.48670/moi-00142 (Accessed on 6-3-2023)
6	Copernicus Climate ERA5 Global climate and weather reanalysis	Hersbach et al., 2018 https://doi.org/10.24381/cds.adbb2d47 (Accessed on 6-3-2023)

486 **Table 1: Products used in the present work. Prod3 is a forcing for Prod1 and Prod6 is a forcing for Prod3. Complete references for**
487 **Prod 1, Prod 3 and Prod. 6 are reported in the bibliography.**

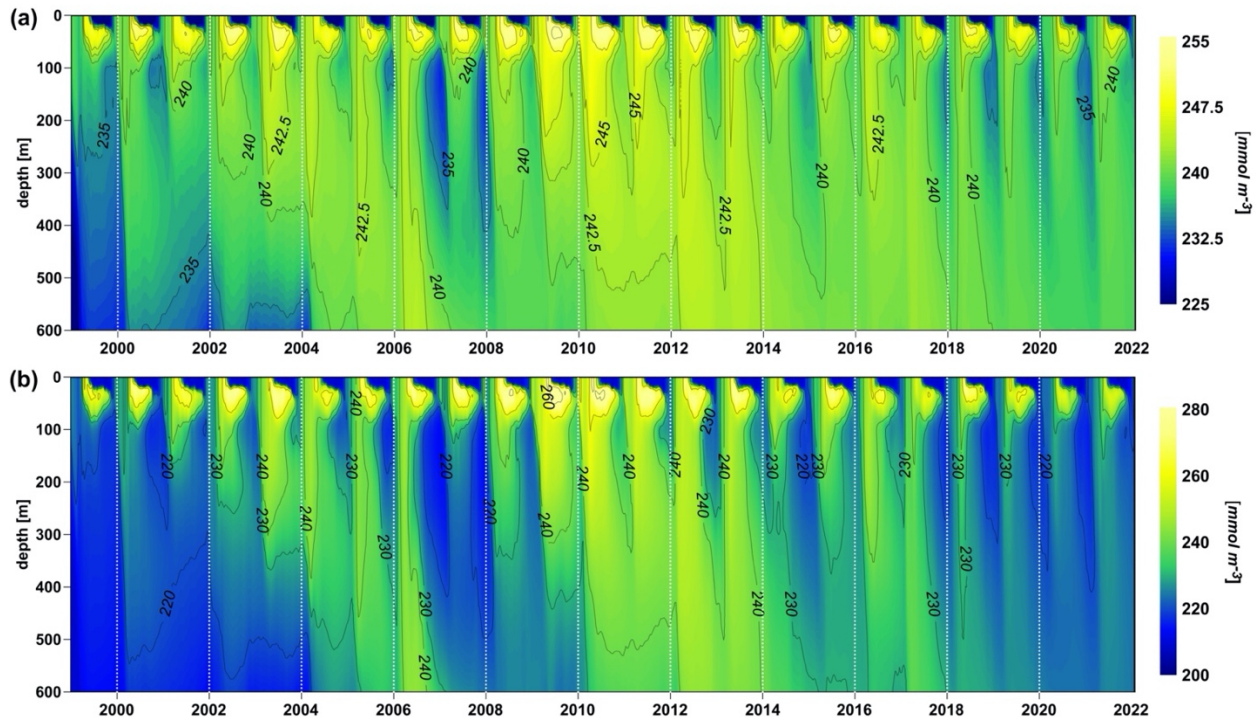
488

489

490

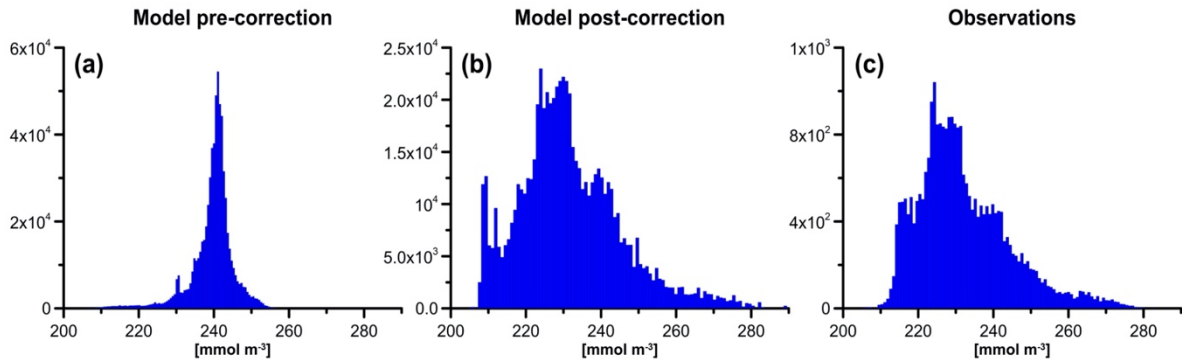
	mode 1	mode 2	mode 3	mode 4
HFlux (SAdr)	0.56	0.15	0.51	0.32
MLD (SAdr)	n.s.	-0.28	-0.41	-0.25
surf chl (SAdr)	n.s.	-0.41	-0.61	n.s.
subsurface chl (SAdr)	0.43	0.13	0.48	0.34
Hflux NAdr (2-months lagged)	n.s.	0.48	0.68	0.16
NIG vorticity (NIon)	n.s.	-0.40	n.s.	-0.37

491 **Table 2: Correlations between the first four temporal modes of EOFs of DO (Figs. 3a,c,e,g) and the forcing fields (Fig. 2, with heat**
492 **fluxes in the northern Adriatic Sea time-lagged by two months). Not statistically significant correlations are identified by a**
493 **significance level higher than 0.05 and indicated by “n.s.” acronym in the table.**



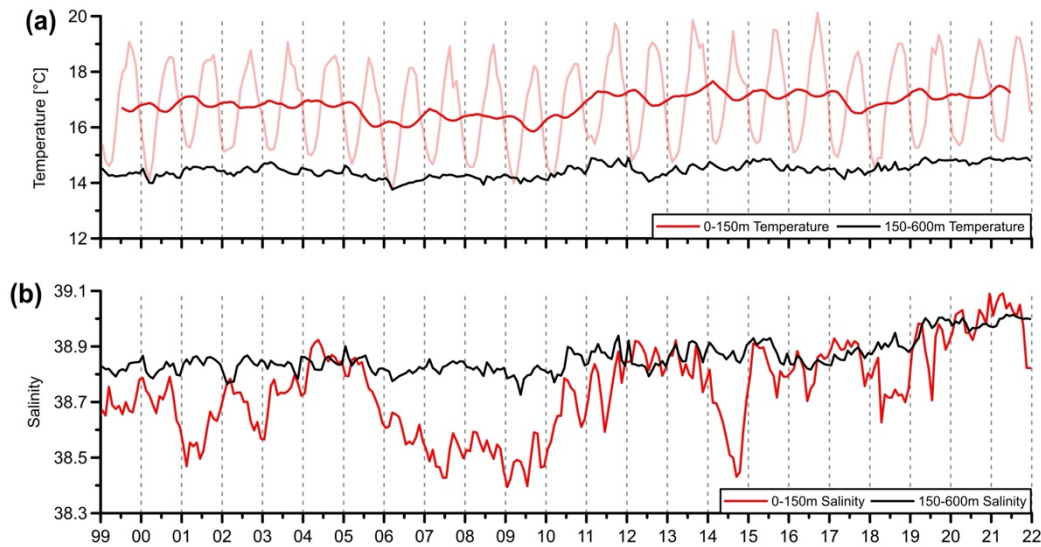
494 **Figure A1: Hovmöller diagram of the modelled oxygen concentrations spatially averaged within the area of autocorrelation equal**
495 **to 0.9 indicated in Fig 1b, before the bias correction by Quantile Mapping (a) and after the procedure (b).**
496

497
498



499

500 **Figure A2:** Frequency histogram of modelled oxygen concentrations before the bias correction by Quantile Mapping (a) and after
501 the procedure (b), compared with BGC-Argo observations (c).
502



503

504 **Figure B1:** Time series of temperature (a) and salinity (b), averaged in the vertical layers 0 - 150 m (red lines) and 150-600 m (black
505 lines) of the Otranto Strait (39.8°N, 18.5° - 19.5° E) in the 1999-2021 time period. In the top panel, light red and dark red indicate
506 data before and after de-seasonalization, respectively. Data are provided by Copernicus physical reanalysis (Prod3, Table 1).
507
508